

Placeholder Name of the conference




Placeholder Session title

<https://doi.org/10.52825/xxxx.....> DOI placeholder (WILL BE FILLED IN BY TIB Open Publishing)

© Authors. This work is licensed under a [Creative Commons Attribution 4.0 International License](https://creativecommons.org/licenses/by/4.0/)

Published: (WILL BE FILLED IN BY TIB Open Publishing)

## RF-sputtered Ti-based dielectric layers as Al-diffusion barrier for passivating contacts

Benjamin Gapp<sup>1</sup>  <https://orcid.org/0000-0002-4620-977X>, Heiko Plagwitz<sup>1</sup>  <https://orcid.org/0000-0003-2869-0149>,  
Giso Hahn<sup>1</sup>  <https://orcid.org/0000-0001-8292-1281>, and Barbara Terheiden<sup>1</sup>

<sup>1</sup> University of Konstanz, Germany

\*Correspondence: Benjamin Gapp, [Benjamin.gapp@uni-konstanz.de](mailto:Benjamin.gapp@uni-konstanz.de)

**Abstract.** We investigate TiN<sub>x</sub> layers deposited via RF magnetron sputtering on their efficacy as a diffusion barrier layer between Al and tunnel oxide passivated contact layer stacks during contact formation in a fast firing process. We obtain implied open-circuit voltage ( $iV_{OC}$ ) from photo-conductance decay measurements in order to analyse the diffusion barrier quality for different parameter variations. In particular, we show the impact of both higher peak temperature and increased thermal budget (by decreasing the slope of the temperature ramp) on  $iV_{OC}$  during the sintering (“fast firing”) process, leading to passivation quality losses.  $iV_{OC}$  losses below 1.5% are shown for peak firing temperatures up to 725°C, with absolute values up to 717 mV after firing. Contact formation at this temperature yields median contact resistivity ( $\rho_c$ ) values below 3 m $\Omega$ cm<sup>2</sup> with a sheet resistance ( $R_{sheet}$ ) of about 40  $\Omega/\square$  for the Ti-based layers.

**Keywords:** Passivating Contact, Aluminum Paste, Diffusion Barrier

### 1. Introduction

Solar cell concepts with passivating contacts, in particular TOPCon cells (cells with tunnel oxide passivated contacts) which allow for high open circuit voltages and therefore conversion efficiencies up to 28.7% [1] (above 26% already achieved [2,3]), rely heavily on the use of Ag electrodes. Considering the limited Ag supply, a large reduction in Ag consumption per Watt produced is necessary to keep up with increasing energy demand and PV deployment roadmaps [4]. This can be achieved with a general Ag reduction (e.g. via electrode geometry adjustment), or by replacing Ag-based metal contacts with an entirely different highly conductive material, such as Al or Cu. Al-based contact setups, in which alloying of Si and Al is typical, have been used extensively in Si-based solar cell concepts (e.g. passivated emitter and rear cells (PERC)) [5,6]. In this work, however, the goal is to prevent this interaction, so as not to impact the phosphorus-doped high-low junction as well as the interface SiO<sub>x</sub> on the Si wafer surface. In order to maintain the surface passivation quality of a passivating contact comprised of SiO<sub>x</sub> and (n)poly-Si:P while still achieving low series resistance contributions from a conventional Al-paste for PERC applications, in this work, a diffusion barrier is introduced. Ti-based layers, such as stoichiometric TiN, have been shown to act as a diffusion barrier against Al up to 550°C [7,8,9] and Si up to 800°C [10] for long durations (30 min). In this work, we investigate Ti-based diffusion barrier layers, deposited with RF magnetron sputtering, enabling contact formation in a fast-firing process while preventing significant passivation losses of the high-low junction.

## 2. Methods

Phosphorus- (10  $\Omega\text{cm}$ ) and boron-doped (1  $\Omega\text{cm}$ ) diamond-wire sawn Czochralski(Cz)-Si wafers were laser cut into 50x50 mm<sup>2</sup> square samples. After saw-damage removal in potassium hydroxide (KOH) at 80°C, the samples were pre-cleaned in an ozone and a piranha-etch solution. Both steps were followed up by a short HF-dip. SiO<sub>x</sub> was then thermally grown in O<sub>2</sub>-atmosphere at 625°C for about 10 min. All wafers were subsequently coated with an amorphous silicon (a-Si) layer (100 nm) on both sides in a plasma-enhanced chemical vapor deposition (PECVD) process comprised of SiH<sub>4</sub>, H<sub>2</sub> and PH<sub>3</sub> for in-situ doping. The a-Si layers were then crystallized in an N<sub>2</sub>-atmosphere at 920°C for 30 min, forming the (n)poly-Si:P layer. After crystallization, the samples were coated on the front side with hydrogenated silicon nitride (SiN<sub>x</sub>:H) in a PECVD process (75 nm). TiN<sub>x</sub> barrier layer deposition (35 nm) on the rear side was then achieved via reactive radio frequency magnetron sputtering from a Ti-target in an Ar-N<sub>2</sub>-plasma (N<sub>2</sub> as reactive gas component for layer formation) at room temperature. In order to prevent further oxidation of the barrier layers during subsequent steps at elevated temperatures, an additional a-Si layer (40 nm) was deposited on samples with (n)poly-Si:P via sputtering without a vacuum-break to create a TiN<sub>x</sub>/(i)a-Si layer stack. Additionally, float-zone(FZ) Si and quartz glass platelets were coated with a TiN<sub>x</sub> single layer as reference samples used for electrical and optical characterization methods. Samples with and without barrier layers were then screen-printed on the rear side with Al paste, dried at 200°C for 400 s. A full-area screen-printing mask was used to contact samples with an n-type base. The samples were then sintered for contact formation in a fast firing process at 700-800°C peak temperature measured on the wafers. The Al metallization of the samples was removed in HCl-solution to enable photo-conductance decay measurements. The samples with p-type base were processed analogously up to printing, where they were selectively printed with an array of 60  $\mu\text{m}$  x 9.5 mm electrodes for measurements, using the transfer-length method in order to determine the impact of the barrier layer on contact resistivity. Each set, consisting of 8 variably spaced electrodes, was printed within 1 of 20 laser-cut areas in order to electrically isolate it from the rest of the sample area. Electrical and optical properties were verified by ellipsometry (fit of layer thickness  $d$  based on Lorentz oscillator models) and four point-probe as well as Hall effect measurements of the Ti-based layer and electrochemical capacitance-voltage (ECV) of the (n)poly-Si:P layers.

## 3. Results

### 3.1 Electrical and optical properties

Fig. 1 depicts electrical and optical properties of TiN<sub>x</sub> layers deposited on FZ-Si and quartz glass platelets of about 20x20 mm<sup>2</sup> at varying plasma conditions. The N<sub>2</sub> content in the gas flow was varied, where  $R_{N_2} = 100\% - R_{Ar}$ . Hall effect measurements were used to obtain charge carrier mobility and bulk concentration of the layers, as shown in Fig. 1(a). The overall high charge carrier concentration combined with high mobility results in a suitably conducting layer ( $R_{\text{sheet}} \sim 40 \Omega/\square$ ) for lateral conductance parallel to the (n)poly-Si:P in a passivating contact. Furthermore, the electrical layer properties can be controlled by the N<sub>2</sub>-content in the gas flow during sputtering. Stoichiometric layers typically present the highest conductivity, which is in line with the data presented in this study [11]. Optical properties were obtained via ellipsometry measurements fitted with a system comprised of one Drude and two Lorentz oscillators, further indicating mostly metallic behaviour of the layers. The high bulk concentration of free charge carriers will give rise to free carrier absorption, further consolidated by the extinction coefficients shown in Fig. 1(b). Only a slight dependence on the N<sub>2</sub> flow during deposition is observed for the  $k$  value (absorption), while the refractive index  $n$  changes more significantly. Generally, the dependence of optical and electrical properties on N<sub>2</sub> flow is expected, since it can be used to influence orientation of the layer and grain size, which in turn are expected to have significant impact on the electrical properties shown [11]. Charge carrier concentrations obtained from Drude model oscillators show similar values to the ones obtained from Hall

measurements, indicating free carrier absorption.

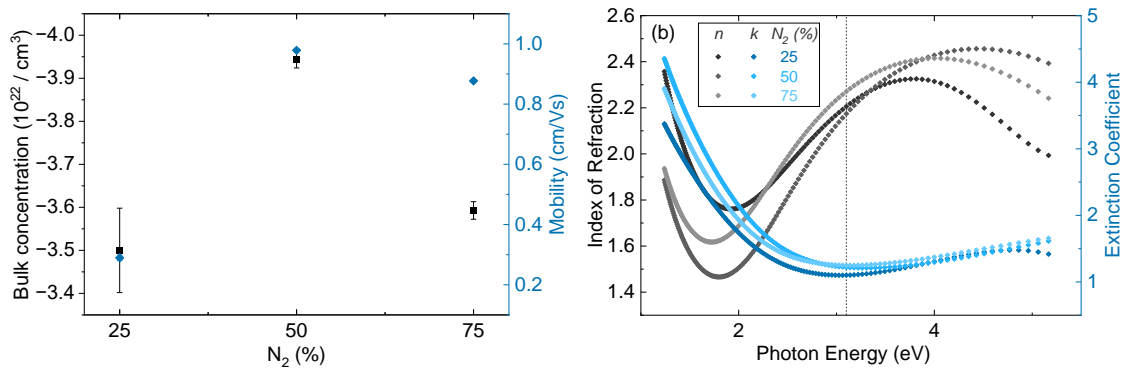


**Figure 1.** (a) Charge carrier concentration, charge carrier mobility and (b) optical constants of reactively sputtered  $\text{TiN}_x$  layers.

### 3.2 Surface Passivation of Passivating Contact with Al Diffusion Barrier

Fig. 2 shows  $iV_{\text{OC}}$  values after typical fast firing contact formation, with and without Al paste applied. Changes in  $iV_{\text{OC}}$  on samples without metallization remain below 10 mV (1.5%) for all samples. For samples with metallization, a direct dependence of the surface passivation losses on the peak firing temperature can be observed. Reference samples with Al metallization and without barrier layers could not be properly measured after firing, likely due to alloying of Al and Si and subsequent massive decrease of the surface passivation. Increasing the thermal budget by decreasing the slope of the temperature ramp during heat up at constant peak temperature leads to larger  $iV_{\text{OC}}$  losses (not shown in Fig. 2). In order to prevent a barrier breakdown at temperatures necessary for contact formation, a steep slope of the temperature ramp is therefore beneficial [12].

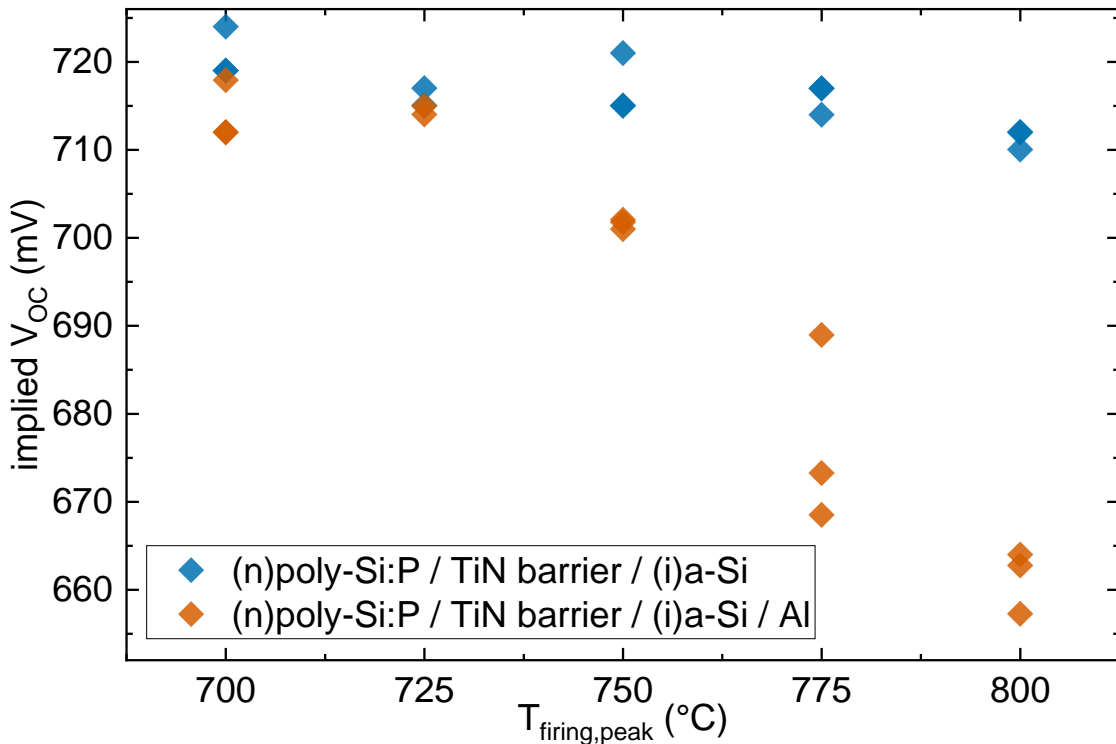


**Figure 2.**  $iV_{\text{OC}}$  measurements for non-metallized and metallized samples for different peak temperatures during fast firing.

### 3.3 Influence of Al Diffusion Barrier on $\rho_c$

Fig. 3 (left) shows contact resistivity values derived from TLM measurements for two similar Al pastes from different manufacturers for PERC solar cell application. Both pastes were screen-printed onto barrier layer protected samples with p-type base, as described in section 2 and yield comparable contact resistivity values, with paste B showing slightly lower values. Both paste systems allow for values around  $1 \text{ m}\Omega\text{cm}^2$ , with median values below  $3 \text{ m}\Omega\text{cm}^2$ . Although the sample structure used in this experiment does not fully comply with standard TLM theory, accompanying finite element simulations of the measurement show that these values are representative for the contact resistivity from the screen-printed Al to the  $\text{TiN}_x$  barrier layer. Sheet resistance extracted from TLM measurements are between  $20\text{-}30 \text{ }\Omega/\text{sq}$ , which is below  $R_{\text{sheet, TiN}_x}$  and  $R_{\text{sheet, poly-Si:P}}$ , and corresponds well to parallel conduction in both layers. If lateral conductivity equally takes places through both the  $\text{TiN}_x$  barrier layer and (n)poly-Si:P, this indicates that the  $\text{TiN}_x$ /(n)poly-Si:P interface does not limit current transport significantly. The  $\text{TiN}_x$  barrier layer seems to be intact after firing at  $725^\circ\text{C}$ , as can be seen from the scanning electron microscopy (SEM) image in Fig. 3 (right). In this particular image, the  $\text{TiN}_x$  barrier thickness was higher ( $\sim 50 \text{ nm}$ ) due to variation during sputtering. The apparent delamination of the barrier as well as the only partial visibility of the (n)poly-Si:P layer is likely a result of the cleaving during sample preparation. No significant inverted pyramid formation could be found for samples coated with the barrier layer.

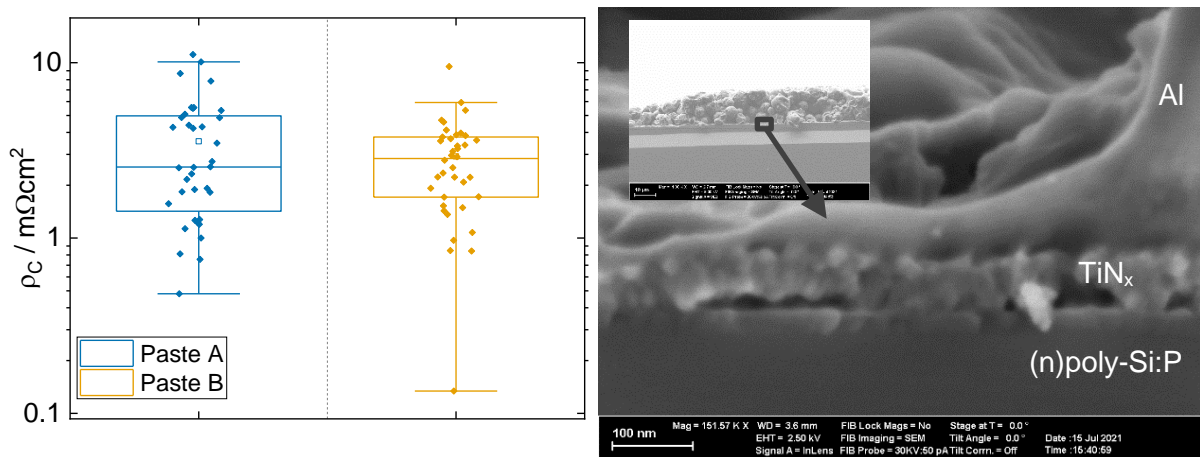


**Figure 3.** Left: Contact resistivity of samples printed with two commercially available Al-pastes directly on the barrier layer for two different pastes, fired at  $725^\circ\text{C}$ . Right: Scanning electron microscopy image of cleaved cross-section of samples with Ti-based diffusion barrier ( $\sim 50 \text{ nm}$ ) and screen printed Al.

## Conclusion

It could be shown that a  $\text{TiN}_x$  layer can be introduced into a passivating contact concept with only minimal detrimental effects on contact resistivity and surface passivation. The efficacy of Ti-based dielectrics as diffusion barrier in passivating contact concepts could be demonstrated. A barrier layer of about  $35 \text{ nm}$  thickness can be used to effectively limit passivation losses due to screen-printing and firing of Al paste up to  $725^\circ\text{C}$  firing temperature during contact formation, with up to  $iV_{\text{OC}} = 715 \text{ mV}$  after firing samples with full-area metallization at  $T_{\text{firing, peak}} = 725^\circ\text{C}$ . A dependence on the firing profile further indicates the diffusion barrier properties of  $\text{TiN}_x$  to be dependent on thermal budget. No inverted pyramids could be found in SEM for samples fired at  $700^\circ\text{C}$ . Median contact resistivity in the applicable peak firing temperature window is shown to be below  $3 \text{ m}\Omega\text{cm}^2$  with barrier sheet resistance as low as  $40 \text{ }\Omega/\square$ .

## Data availability statement

The data that support the findings of this study and details on the measurement setup are available from the corresponding author upon reasonable request.

## Author contributions

**Benjamin Gapp:** Investigation, Conceptualization, Formal analysis, Writing - Original Draft  
**Heiko Plagwitz:** Investigation, Conceptualization, Supervision, Review, Editing  
**Giso Hahn:** Review, Editing, Supervision  
**Barbara Terheiden:** Conceptualization, Supervision, Resources, Funding acquisition, Project administration

## Competing interests

The authors declare that they have no competing interests.

## Funding

Part of this work was financially supported by the German Federal Ministry for Economic Affairs and Climate Action (FKZ 03EE1106B). The content is the responsibility of the authors.

## Acknowledgement

The authors would like to thank Barbara Rettenmaier for technical support.

## References

- [1] W. Long, S. Yin, F. Peng, M. Yang, X. Ru, M. Qu, H. Lin, X. Xu, "On the limiting efficiency for silicon heterojunction solar cells", *Solar Energy Materials and Solar Cells*, 231, 111291, 2021, doi: <https://doi.org/10.1016/j.solmat.2021.111291>
- [2] M.A. Green, E.D. Dunlop, J. Hohl-Ebinger, M. Yoshita, N. Kopidakis, X. Hao, "Solar cell efficiency tables (version 57)." *Progress in photovoltaics: research and applications* 29, 1, pp. 3-15, 2021, doi: <https://doi.org/10.1002/pip.3371>
- [3] F. Haase, C. Hollemann, S. Schäfer, A. Merkle, M. Rienäcker, J. Krügener, R. Brendel, R. Peibst, "Laser contact openings for local poly-Si-metal contacts enabling 26.1%-efficient POLO-IBC solar cells." *Solar Energy Materials and Solar Cells* 186, pp. 184-194, 2018, doi: <https://doi.org/10.1016/j.solmat.2018.06.020>
- [4] Y. Zhang, M. Kim, L. Wang, P. Verlinden, B. Hallam, "Design considerations for multi-terawatt scale manufacturing of existing and future photovoltaic technologies: challenges and opportunities related to silver, indium and bismuth consumption", *Energy & Environmental Science* 14, 11, pp. 5587-5610, 2021, doi: <https://doi.org/10.1039/D1EE01814K>
- [5] G. Fischer, M. Müller, S. Steckemetz, R. Köhler, F. Lottspeich, F. Wolny, C. Koch, T. Roth, M. Kipping, H. Neuhaus, E. Schneiderlöchner, "Model based continuous improvement of industrial p-type PERC technology beyond 21% efficiency", *Energy Procedia*, 77, pp. 515-519, 2015, doi: <https://doi.org/10.1016/j.egypro.2015.07.073>
- [6] A. Metz et al., "International Technology Roadmap for Photovoltaic (ITRPV) 2014 Results".
- [7] M. Wittmer, "Properties and microelectronic applications of thin films of refractory metal nitrides", *Journal of Vacuum Science & Technology A: Vacuum, Surfaces, and Films*, 3, 4, pp. 1797-1803, 1985, doi: <https://doi.org/10.1116/1.573382>

- [8] A. Sherman, "Growth and properties of LPCVD titanium nitride as a diffusion barrier for silicon device technology", *Journal of the Electrochemical Society* 137, 6, pp. 1892-1897, 1990, doi: <https://doi.org/10.1149/1.2086826>
- [9] G.I. Grigorov, K.G. Grigorov, M. Stoyanova, J.L. Vignes, J.P. Langeron, P. Denjean, "Aluminium diffusion in titanium nitride films. Efficiency of TiN barrier layers", *Applied Physics A*, 57, pp. 195-197, 1993, doi: <https://doi.org/10.1007/BF00331444>
- [10] K.G. Grigorov, G.I. Grigorov, M. Stoyanova, J.L. Vignes, "Diffusion of silicon in titanium nitride films. Efficiency of TiN barrier layers", *Applied Physics A*, 55, 5, pp. 502-504, 1992, doi: <https://doi.org/10.1007/BF00348340>
- [11] Arshi, N., Lu, J., Joo, Y. K., Lee, C. G., Yoon, J. H., Ahmed, F., "Study on structural, morphological and electrical properties of sputtered titanium nitride films under different argon gas flow", *Materials Chemistry and Physics*, 134(2-3), 839-844, 2012, doi: <https://doi.org/10.1016/j.matchemphys.2012.03.078>
- [12] H.J. Lee, R. Sinclair, P. Li, B. Roberts, "A study of the failure mechanism of a titanium nitride diffusion barrier", *Journal of Applied Physics*, 86, 6, pp. 3096-3103, 1999, doi: <https://doi.org/10.1063/1.371173>